Catalysis
Science & Technology

RSC Publishing

PAPER

View Article Online
View Journal | View Issue

Cite this: *Catal. Sci. Technol.*, 2013, **3**, 2819

A mild solution chemistry method to synthesize hydrotalcite-supported platinum nanocrystals for selective hydrogenation of cinnamaldehyde in neat water†

Xu Xiang,*[a] Wanhong He,[ab] Lisha Xie[a] and Feng Li[a]

Received 25th June 2013,
Accepted 31st July 2013

DOI: 10.1039/c3cy00437f

www.rsc.org/catalysis

Hydrotalcite-supported platinum nanocrystals (Pt NCs) were synthesized by a facile solution chemistry method, and then applied as an efficient catalyst for the selective hydrogenation of cinnamaldehyde (CMA) in neat water. The reduction of metal precursor ions was achieved in an aqueous solution at a low temperature (323 K), simultaneously accompanied by the crystallization of the hydrotalcite support. The size of the Pt NCs can be delicately tuned by the relative ratio of surfactant to metal precursor ions, and characterized by HRTEM and CO-adsorption infrared spectroscopy. The Pt particle sizes are closely associated with the hydrogenation selectivity toward cinnamyl alcohol (CMO), with a higher selectivity up to 85% over the larger-sized Pt in an aqueous medium. The effects of alkali (NaOH) on the catalytic performance were explored. The findings indicated that the addition of alkali enhances the selectivity toward CMO (to 90%). The catalysts showed high stability with a marginal decrease in activity and selectivity after repeated use. The hydrogenation products could be easily separated from the solvent by simple extraction, which is a greener and more convenient process than those using organic solvents.

Introduction

Chemoselective hydrogenation of α,β-unsaturated aldehydes (UALs) or ketones (UKEs) to the corresponding allylic alcohols is of great importance to the synthesis of fine chemicals, such as pharmaceuticals, foods and cosmetics.[1,2] Selective hydrogenation of cinnamaldehyde (CMA) to cinnamyl alcohol (CMO) is a representative of such a class of reactions. Two competitive products of selective hydrogenation can be produced through the hydrogenation of the conjugated C=C or C=O bond over the supported metal catalysts.[3,4] The hydrogenation of C=C *versus* C=O in the conjugated aldehydes and ketones is thermodynamically favorable of the former because of the significantly higher activation barriers to hydrogenate the C=O bond compared with those required to hydrogenate the C=C bond.[5] Generally, the challenge is associated with the hydrogenation of the C=O bond to the desired unsaturated alcohol without reacting the C=C bond.[6] Common noble metals like Pt,[7,8] Pd[9–11] and Ru[12] presented an intrinsically higher selectivity toward the C=C bond to produce a saturated aldehyde. Hence, great efforts have been made to enhance their selectivity either by fine control of the sizes[13] and/or the exposed facets of the active metal nanoparticles,[14] or by decorating the primary metal with a second metal component.[15–20] Also, modification of the supports[21–24] or the addition of a promoter (Lewis acids or bases)[8] are alternative ways to tune the selectivity. Biocatalytic routes have also been explored as alternatives for the selective reduction in recent years.[25] Although most of these strategies are proven effective, the preparation of catalysts is usually tedious and complicated or less environmentally friendly. A facile and mild approach for obtaining supported metal catalysts capable of high activity and selectivity is highly desirable.

In addition to the catalyst preparation, the increasing concerns around environmental issues in the past decade, have promoted the progress of metal-catalyzed liquid-phase reactions achieved in an aqueous medium or "on water".[26,27] It is generally accepted that one of the key principles of green chemistry is the elimination of solvents in chemical processes or the replacement of hazardous solvents with environmentally benign solvents like water.[28] Regarding the liquid-phase

[a] *State Key Laboratory of Chemical Resource Engineering, Beijing University of Chemical Technology, Beijing, 100029, China. E-mail: xiangxu@mail.buct.edu.cn; Fax: +86-10-64425385; Tel: +86-10-64412109*

[b] *Key Laboratory of Fine Petrochemical Engineering of Jiangsu Province, Changzhou, 213164, P.R. China*

† Electronic supplementary information (ESI) available: Effect of solvents; TEM photographs; FTIR spectra, XRD pattern and XPS spectra of the catalyst after use. See DOI: 10.1039/c3cy00437f

hydrogenation of UALs, the catalytic reactions were often carried out in organic media (alcohol, cyclohexane or toluene *et al.*),[29] increasing the risk of environmental hazards and the complexity of product separation. There are few reports on the hydrogenation of UALs over supported catalysts in an aqueous medium,[5,30] even though there are potential advantages in its green and environmental friendly approach. Very recently, Cao *et al.* demonstrated that gold supported on mesostructured ceria can catalyze the reduction of UALs and UKEs to the corresponding allylic alcohols in high yields in an aqueous medium,[31] which established a green protocol for chemoselective conversion of UALs to a desired unsaturated alcohol product.

Inspired by this pioneering work, herein, we synthesized hydrotalcite-supported platinum nanocrystals (Pt NCs) by a mild and facile method, which were used as catalysts for selective hydrogenation of cinnamaldehyde in neat water. The preparation process integrates the reduction of the metal precursor, the deposition of the Pt NCs and the crystallization of the support into one process (*all-in-one*). The hydrotalcite, also known as MgAl-layered double hydroxide (MgAl-LDH) with a formula of $Mg_6Al_2(OH)_{16}CO_3{\cdot}nH_2O$, consists of a positively-charged brucite-like layer and charge-balanced anions within the interlayer gallery. MgAl-LDH has extensively been used to support noble metals and been applied in a variety of catalytic reactions.[32–34] The hydroxyl group in the structure of hydrotalcite may inhibit the adsorption of the C=C bond by electrostatically repelling the phenyl ring of cinnamaldehyde without the need of a foreign promoter (*e.g.* an alkali). Also, the hydrophilicity of hydrotalcite could be beneficial to the orientation of the hydrophilic C=O moiety on the surface active sites of the catalyst.

The supported Pt catalysts exhibited high selectivity toward the C=O bond (85% selectivity), which is closely related to the size of the Pt NCs. The larger Pt NCs resulted in higher selectivity toward the cinnamyl alcohol (CMO). The high activity and selectivity could be retained in the third recycle. In particular, the products could be easily separated from the aqueous medium after the reaction by extraction since water was used as a green solvent. No organic solvents or toxic agents were used throughout either the preparation of the catalysts or the catalytic reactions. This current study, for the first time, explores a green process for the hydrogenation of cinnamaldehyde over highly efficient hydrotalcite-supported Pt catalysts using neat water as a reaction medium.

Results and discussion

Characterization of the catalysts

The catalysts were prepared with an initial ratio of TTAB (tetradecyl trimethyl ammonium bromide) to Pt^{4+} of 25 : 1, 50 : 1 and 100 : 1 denoted as Pt/MA-1, Pt/MA-2 and Pt/MA-3, respectively. The same procedure was carried out without the addition of TTAB and the catalyst was denoted as Pt/MA (Table S1 in the ESI†). Also, the MgAl-LDH without the loading of Pt was synthesized under the same conditions and denoted as MA.

The supported Pt catalysts were synthesized by an aqueous nanochemistry method under mild conditions (323 K). The Pt^{4+} ions were reduced to metallic Pt nanocrystals using the reducing agent $NaBH_4$, simultaneously accompanied by the aging of the hydrotalcite support. The phase structure and composition of the catalysts were confirmed by XRD. The patterns of MA with no loading of Pt showed characteristic diffractions of hydrotalcite (Fig. 1a), which agrees well with the reported results (JCPDS Card No. 89-0460). The (00*l*) diffractions in low angles indicate its layered structure. The d_{003} basal spacing is ~7.6 Å, suggestive of the intercalation of carbonate ions as compensating anions. The Pt NCs supported on hydrotalcite exhibit the same diffractions to that of hydrotalcite (Fig. 1b–e). The diffraction of d_{003} shows little shift compared to the support itself. This indicates that the layered hydrotalcite is not intercalated by $PtCl^{4-}$ anions during the reaction. It is reasonable as carbonate anions are prone to intercalate and stable in the interlayer galleries in the carbonate-containing solution.

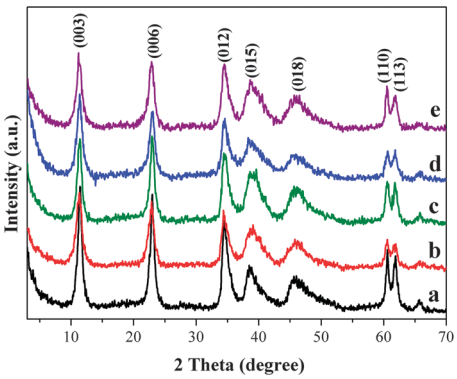

Fig. 1 Powder XRD patterns of hydrotalcite-supported Pt catalysts: (a) MA, (b) Pt/MA, (c) Pt/MA-1, (d) Pt/MA-2, (e) Pt/MA-3.

Besides the characteristic diffractions corresponding to the layered structure of hydrotalcite, the diffractions associated with metal Pt or other Pt species are not observed. This can be attributed to the high dispersion of the Pt NCs of small sizes and/or the low loading of Pt (~1.96 wt%). It has been reported that supported Pt or Pd nanoparticles are located mostly on the surface or the edge-on sites of the hydrotalcite rather than in the interlayer space.[32,34]

The reduction of the metal precursor was mediated by the surfactant TTAB during the synthesis. It was reported that surfactant residues in catalysts may poison the active sites.[35] Therefore, FTIR analyses were carried out to detect possible residues of surfactant in the as-synthesized catalysts. The IR spectra of Pt/MA (with no addition of TTAB) and Pt/MA-3 (with a maximal quantity of TTAB added) were compared (Fig. 2). A broad absorption band in the range of 3600–3200 cm^{-1} centered at 3468 cm^{-1} corresponds to the O–H stretching vibrations (ν_{OH}) of the hydroxyl groups in the brucite-like layers and interlayer water molecules. The absorption bands peaked at 1376 cm^{-1} and 855 cm^{-1} are attributable to the symmetric stretching vibrations (ν_3) and out-of-plane deformation (ν_2) of the carbonate ions, suggestive of the presence of interlayer carbonate anions.[36] The weak absorption at 1643 cm^{-1} is assigned to the bending vibration of interlayer water (δ_{OH}). The bands in the lower frequency region, around 660–580 cm^{-1}, are

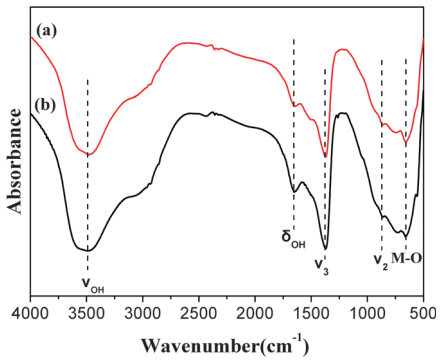

Fig. 2 FTIR spectra of the supported Pt catalysts: (a) Pt/MA, (b) Pt/MA-3.

attributed to metal–oxygen (M–O) and metal–hydroxyl (M–OH) vibrations in the lattice of the hydrotalcite. There is no detectable difference between the two spectra, indicative of the absence of any residues associated with TTAB. It was reported that the bromide-mediated strategy is more favorable catalytically because the bromide species are only on the nanocrystal surface and are easily removed after synthesis by washing.[37] The results of the IR analyses clearly suggest that the TTAB species have been efficiently removed from the surface of the catalysts by repeated washing.

The reduction of the metal precursors was achieved by a surfactant-mediated solution synthesis. It was expected that the sizes or morphologies of the Pt NCs could be tuned by the kinetics-controlled reduction by the surfactant. The particle sizes and morphology of the reduced Pt NCs were studied by HRTEM. Fig. 3 shows TEM photographs of a series of Pt catalysts. It is observed that Pt NCs are highly dispersed on the support regardless of the addition of the surfactant. However, the Pt sizes present an obvious difference for these catalysts. The Pt/MA catalyst has smaller Pt NCs with a mean size of 2.3 nm and a wider size distribution (Fig. 3a). While the metal precursor was reduced in the presence of the surfactant (TTAB), the Pt NCs show larger sizes and a narrower size distribution (Fig. 3b–d). Furthermore, the particle sizes is dependent on the quantity of TTAB. The higher the ratio of TTAB to metal precursor, the smaller the size of the Pt NCs (varying from 5.0, 4.0 to 3.4 nm).

This finding could be explained by the role of TTAB as a stabilizing agent in controlling the reduction kinetics of the metal precursor. The reducing agent $NaBH_4$, has robust reduction ability. The Pt^{4+} ions can be instantaneously reduced upon the addition of $NaBH_4$, which was witnessed by the rapid color change of the solution from bright-yellow to black. The reduction of Pt^{4+} ions slightly slowed down in the presence of TTAB and the color changed to light black, resulting from the change of local micro-environment around Pt^{4+} ions and the stabilizing role of TTAB. It has been reported that the sizes of Pt NCs could be tuned by controlling the reducing rate of the metal precursor ions in a polyol synthesis.[37] The faster nucleation rate leads to the smaller Pt nanoparticles, while the slower nucleation and growth gives rise to bigger ones. In this work, the size of the Pt NCs could be tuned by reduction and/or

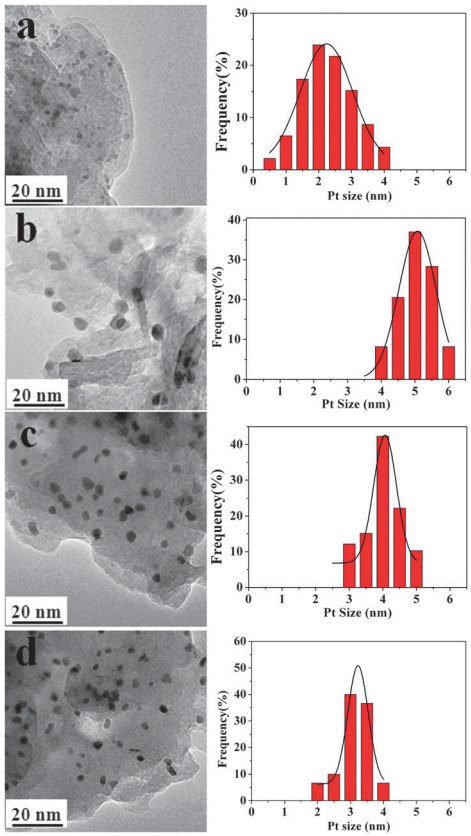

Fig. 3 TEM photographs of the supported Pt catalysts: (a) Pt/MA, (b) Pt/MA-1, (c) Pt/MA-2, (d) Pt/MA-3. Pt size distribution histograms were shown in the right column.

growth kinetics. It is interesting that the size of the Pt NCs decreases with increasing quantity of TTAB. We are not sure whether more TTAB promotes an accelerated nucleation, leading to a decrease in Pt size at present. Nevertheless, it is clear that the supported Pt NCs have tunable sizes, suitable for a size-dependent study in catalysis.

HRTEM observations were carried out to further reveal the microstructure of the Pt NCs. As to Pt/MA (Fig. 4a), the lattice image displays an interplanar spacing of 0.226 nm, corresponding to the plane Pt{111}. The Pt NCs show a poor contrast with the support, suggestive of a low degree of crystallization. Such a structure could cause a high occupancy of defective and low-coordinated sites on the surface of the Pt. The Pt NCs for Pt/MA-1 and Pt/MA-2 exhibit a quasi-cuboctahedral shape with clear boundaries (Fig. 4b and c). The previous study reported the control of the shape of free-standing Pt nanoparticles by a bromine-mediated method.[38] In our case, both the size and shape of supported Pt NCs can be tuned by a stabilizing agent TTAB during the synthesis. The cuboctahedral shape results in a predominance of plane {111} in the exposed facets of Pt. With further increasing the quantity of TTAB, the Pt NCs appear spherical or ellipsoidal in shape with a smaller size (Fig. 4d). As a result, the shape evolution causes an average of exposed facets and no specific facets are predominant in this catalyst. The catalytic hydrogenation of unsaturated aldehyde could be

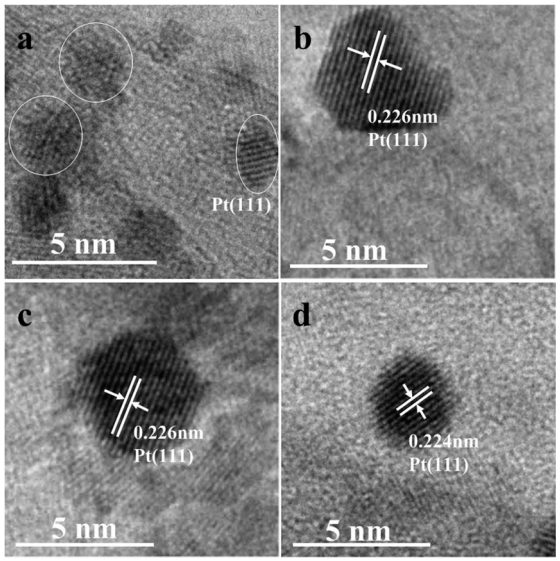

Fig. 4 HRTEM images of the supported Pt catalysts: (a) Pt/MA, (b) Pt/MA-1, (c) Pt/MA-2, (d) Pt/MA-3. The Pt NCs were highlighted by white circles in (a); the interplanar spacing of Pt{111} labelled in (b), (c) and (d).

size- or shape-sensitive to the metal nanoparticles.[14,39] Consequently, it is expected that these catalysts may demonstrate different activity and selectivity in cinnamaldehyde hydrogenation.

To study the chemical valence of elements in the Pt catalysts, XPS characterization was carried out. For all four catalysts, the core level spectra can be fitted with three contributions (Fig. 5). The component at 74.7 ± 0.1 eV is assigned to the Al2p level, resulting from the hydrotalcite (Table 1). The other two contributions come from the spin–orbit components $Pt4f_{7/2}$ and $Pt4f_{5/2}$, respectively, peaked at 70.9 ± 0.1 eV and 74.1 ± 0.1 eV, which is assigned to zerovalent Pt^0 in the metallic state.[24,40] The spin orbital splitting shows the same value ~3.2 eV, which agrees well with reports in the literature.[40] No contributions associated with Pt^{2+} or Pt^{4+} species are observed in the XPS spectra. The results suggest that the amount of TTAB added has little effect on the reduction of Pt^{4+} although it has a

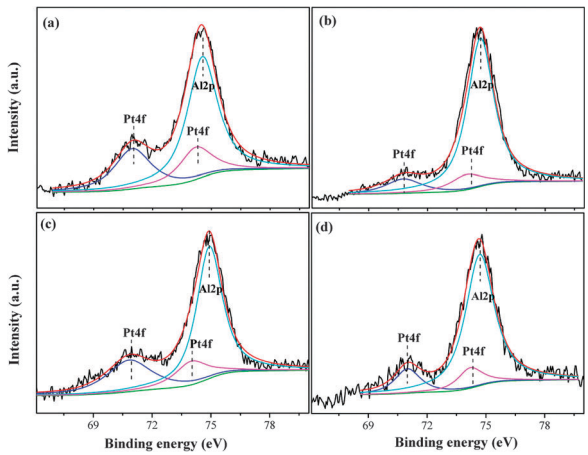

Fig. 5 XPS spectra of Pt4f core level in the supported catalysts: (a) Pt/MA, (b) Pt/MA-1, (c) Pt/MA-2, (d) Pt/MA-3.

Table 1 XPS binding energy of Pt4f core levels in the supported catalysts

Catalysts	$Pt4f_{7/2}$	$Pt4f_{5/2}$	Ratio[b]
Pt/MA	71.0(2.2)[a]	74.2(2.0)	1.40
Pt/MA-1	70.9(2.4)	74.1(2.2)	1.35
Pt/MA-2	70.8(2.2)	74.0(2.0)	1.39
Pt/MA-3	71.0(2.2)	74.2(2.0)	1.36

[a] The Full-Width Half-Maximum (FWHM) values are listed in parentheses. [b] The ratio of integral peak area of $Pt4f_{7/2}$ to $Pt4f_{5/2}$, close to a value of 4 : 3.

remarkable effect on the size of the Pt NCs. In addition, the XPS results confirm that the metal–support interaction hardly affects the electronic levels of the Pt species as there is no observable B.E. shift among these catalysts (Table 1).

To further address the size or surface effect of the Pt catalysts, the catalysts were examined using a probe molecule *i.e.* CO, which was adsorbed onto the Pt surface and was subsequently studied by infrared spectroscopy. Fig. 6 shows the FTIR spectra of CO adsorbed onto a series of Pt catalysts. The IR spectra recorded display two distinctive $\upsilon_{C=O}$ vibration bands. The first in the range of 2060–2030 cm^{-1} is assigned to linearly adsorbed CO molecules on a single Pt atom site. The second between 1830–1860 cm^{-1} displays a broad and weak peak, attributable to bridging CO on two or more Pt atoms.[41] The results indicate that Pt adsorbs CO predominantly in a linear way, with a low occupancy of bridged sites at high CO coverage. It is found that the $\upsilon_{C=O}$ linear mode shows a red shift with decreasing size of the Pt NCs. Similar findings have also been observed in mono- and bi-metallic Pt catalysts.[39,41] The maximal size (5.0 nm) of Pt gives rise to a peak appearing at 2051 cm^{-1}, while the Pt NCs with a mean size of 2.3 nm make the linear mode redshift to 2031 cm^{-1}.

It is known that smaller Pt particles contain more low-coordinated surface sites and the larger particles have increasing occupancy of flat surfaces. The CO-adsorption results indicate that the exposed Pt atom bearing a CO ligand experiences an increasing degree of back-bonding of its d-electrons (increasing δ^- on the Pt surface) to the π^* of the CO molecules, when the size of Pt is larger.[39] The increasing δ^- of the Pt atoms destabilizes the adsorption of the C=C bond and thus enhances the selectivity

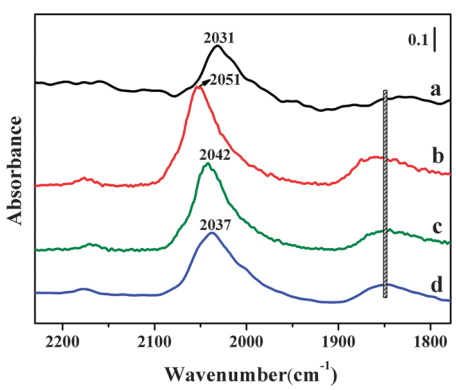

Fig. 6 FTIR spectra of CO adsorbed on the Pt catalysts at room temperature: (a) Pt/MA, (b) Pt/MA-1, (c) Pt/MA-2, (d) Pt/MA-3.

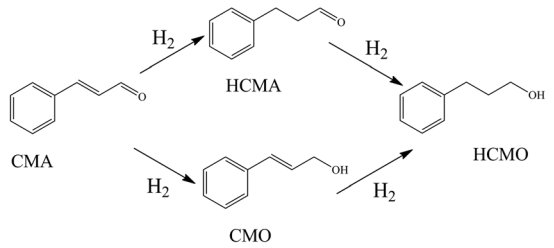

Scheme 1 The reaction pathway and main products for hydrogenation of cinnamaldehyde (CMA).

toward CMO (C═O hydrogenation). The bridging absorption of CO in the 1830–1860 cm^{-1} shows little difference for the Pt catalysts synthesized in the presence of the surfactant (Fig. 6b–d). In contrast, this bridging mode presents a weaker band on the Pt/MA (in the absence of TTAB during the synthesis). It may be attributable to more bridged sites being accessible to larger and better-crystallized Pt NCs.

Hydrogenation of cinnamaldehyde over the Pt catalysts

Scheme 1 shows the reaction pathway and main products for the hydrogenation of cinnamaldehyde. The hydrogenation of C═C *versus* C═O in conjugated aldehydes is thermodynamically in favor of the former. Recently, Corma *et al.* found that H_2 dissociation on Pt nanoparticles is considerably faster than that on Au, because H_2 adsorption on Pt atoms is dissociative and no activation barriers are involved. The high chemoselectivity of Au/TiO_2 catalysts does not exist in Pt/TiO_2 catalysts no matter how small the Pt particles are.[42] Hence, it is more challenging to enhance the selectivity toward C═O bond to produce the desired unsaturated alcohol (CMO) over the supported Pt catalysts. Here, the catalytic hydrogenation of cinnamaldehyde was achieved using water as a medium under relatively mild reaction conditions (1 MPa H_2, 333 K).

The catalytic performance of cinnamaldehyde hydrogenation over the supported Pt catalysts are listed in Table 2. The dispersion was estimated from the mean Pt particle size assuming cuboctahedrally shaped metal particles.[10] The initial turnover frequency (TOF) was applied to estimate the kinetics of the catalytic reactions. They are calculated at CAL conversion of approximately 10% in order to get the intrinsic kinetics.[30] The TOF reach 0.488 s^{-1} over the Pt/MA-1 catalyst, higher than such Pt catalysts on carbon or common oxide supports under similar reaction conditions.[14,18,24] The catalysts with smaller sizes of Pt NCs present a decrease in TOF owing to a higher dispersion (Pt/MA and Pt/MA-3). It is noted that the selectivity toward CMO is closely associated with the Pt particle size. The selectivity reaches 85% (CMO yield of 68%) under a high conversion of ~80% over the Pt/MA-1 catalyst (5.0 nm Pt). Besides, the complete hydrogenation toward HCMO is almost negligible (1%). With a decrease in Pt size, the selectivity toward CMO decreases and increases towards HCMA and HCMO. This suggests that the small-sized Pt favors the adsorption of the C═C bond due to the abundance of low-coordinated surface sites, which is consistent with the results of the CO-adsorption IR. The size-dependence of hydrogenation selectivity on the Pt catalysts has also been found in the previous studies.[13,39]

In addition, the morphology effect cannot be neglected. The Pt/MA catalyst showed a remarkably lower selectivity toward CMO compared to the other catalysts. This could partly be explained by its high occupancy of defective sites on the surface, resulting from the low degree of crystallinity. The abundance of exposed flat facets in the Pt/MA-2 and Pt/MA-3 (see HRTEM in Fig. 4) increases the repulsive interaction with the phenyl ring in cinnamaldehyde, leading to the carbonyl group (C═O) aligning with the surface as a head-on attack. However, it is quite difficult to further enhance the selectivity toward the C═O bond as the dynamic adsorption of the unsaturated aldehyde on the remaining terrace sites of the larger Pt NCs cannot be completely inhibited.

The nanochemistry synthesis in the mild reaction conditions makes the smaller Pt NCs contain higher proportions of defective and low-coordinated metal surface sites. The increasing occupancy of the low-coordination surface sites by smaller-sized Pt could explain the decrease in hydrogenation selectivity. In comparison, the larger-sized Pt NCs contain a higher proportion of flat surfaces with a smaller occupancy of defective surface sites. This leads to an enhancement in the selectivity. Besides, the current work could be more advantageous over previous studies because of the two following merits. Firstly, the synthesis of Pt catalysts was performed by a mild solution chemistry method, which avoids tedious or unfriendly involvement of organic solvents and/or high temperature post-treatments. Secondly, the catalytic reactions were carried out using neat water as a medium, representative of a greener process and providing a facile separation after the reaction by simple extraction.[31]

Table 2 The size of the Pt nanocrystals and their catalytic performance for hydrogenation of cinnamaldehyde

						Selectivity[d] (%)		
Catalysts	Pt size (nm)	Dispersion[a] (%)	TOF[b] (s^{-1})	Conversion (%)	Yield[c] (%)	CMO	HCMA	HCMO
Pt/MA	2.3	49.1	0.270	91.1	45.6	50.1	35.6	13.9
Pt/MA-1	5.0	22.6	0.488	79.7	68.0	85.4	13.3	1.0
Pt/MA-2	4.0	28.2	0.410	84.3	64.5	76.6	17.3	5.6
Pt/MA-3	3.4	33.2	0.363	87.2	61.4	70.5	20.4	8.7

[a] Estimated from TEM results (the mean Pt particle size). [b] TOF was calculated at CMA conversion of approximately 10%. [c] Yield of CMO. [d] Selectivity was reported at the level of conversion in the table. Reaction conditions: 0.05 g catalyst, substrate: 4 mmol CMA, solvent: 15 mL water, H_2 pressure: 1.0 MPa, temperature: 333 K, reaction time: 2 h.

In contrast, the catalytic reactions were carried out using common organic solvents to reveal the effects of the solvent on catalytic performance. It is found that the activity and CMO selectivity in ethanol and isopropanol are slightly higher than those in water, while the activity and selectivity dramatically decreases in cyclohexane (Table S2 in the ESI†). However, other products increase to ~5% when using ethanol or isopropanol as a solvent compared to a negligible value (0.3%) using water as a solvent. Other products mainly include acetals, resulting from the effect of solvent. Therefore, using water as a green solvent can effectively inhibit the formation of other products like acetals.

The slightly higher activity and selectivity in ethanol and isopropanol could be attributable to the polarity of the solvents and the solubility of H_2. There is a comparable polarity in ethanol and isopropanol, while water has a stronger polarity (Table S3 in the ESI†). It has been reported that the water-assisted orientation of hydrophilic C=O moiety on the active sites favored chemoselective hydrogenation.[7,43] Hence, water could be a beneficial solvent than organic ones. However, the solubility of H_2 in ethanol and isopropanol is four times higher than that in water. It could be a decisive factor to affect the activity of hydrogenation due to the dissociative characteristic of H_2-adsorption on Pt atoms. The present findings with Pt catalysts differ from those with Au/CeO_2 catalysts, in which higher activity was obtained when using water as a medium than those using organic solvents.[31]

The time course of CMA conversion and selectivity over the catalyst Pt/MA-1 was investigated (Fig. 7). In neat water, the CMA conversion reaches ~80% after 2 h and the selectivity to CMO keeps almost unchanged (~85%). To further extend the reaction time to 2.5 h, the conversion increases to ~90%, while the selectivity toward CMO decreases to 80% and the amount of HCMO obviously increases. It is concluded that CMO is prone to transform into HCMO (complete hydrogenation) under high conversion (>90%). This is a strong indication that CMO is less thermodynamically stable compared to its competitive product HCMA.[44] Consequently, it is more challenging to obtain CMO than HCMA by a selectivity-controlled hydrogenation.

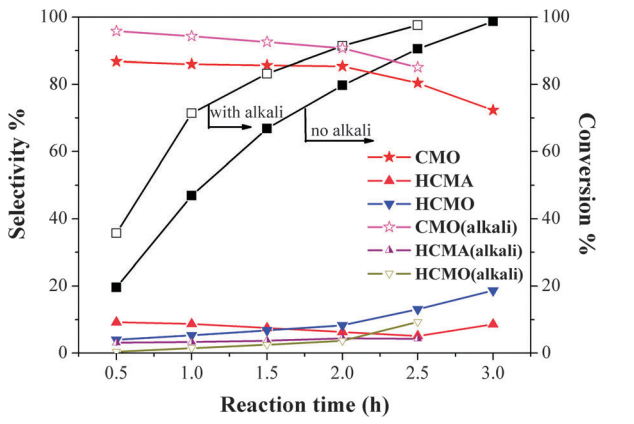

Fig. 7 Evolution of CMA conversion and selectivity in neat water over the catalyst Pt/MA-1. CMA conversion (solid square), CMA conversion with the addition of alkali (empty square); CMO selectivity (solid star), HCMA selectivity (solid up triangle), HCMO selectivity (solid down triangle); with the addition of alkali: CMO selectivity (empty star), HCMA selectivity (half-empty up triangle), HCMO selectivity (empty down triangle). Reaction conditions: 0.05 g catalyst, substrate: 4 mmol CMA, solvent: 15 mL water, H_2 pressure: 1.0 MPa, temperature: 333 K.

It has been reported that the alkali promoter was able to modify the adsorption mode of cinnamaldehyde and thus change the selectivity to a desired product. Lin *et al.* found that the addition of KOH enhanced the selectivity to CMO (77–83% at a CMA conversion of 49–74%).[8] The electropositive alkali metal ions such as K^+ or Na^+ can activate the C=O bond by a robust interaction with the lone pair of electrons in the oxygen of carbonyl group.[45,46] Nearby OH^- ions could inhibit the adsorption of C=C bond by electrostatically repelling the phenyl ring of cinnamaldehyde. The hydrogen atom adsorbed on the Pt atom is favorable to attack and hydrogenate the C=O bond. In our work, indeed, we found that the addition of alkali (NaOH) promoted the selectivity toward CMO (91% at 2 h, CMO yield of 82%). Besides this, the selectivity reduces with increasing conversion after a reaction time of 2 h (Fig. 7). This trend is consistent with that without addition of alkali.

The effects of the reaction temperature was also explored. The CMA conversion shows an increasing trend with elevating reaction temperature (Table 3). The selectivity toward CMO presents a reverse tendency. The higher selectivity is achieved (~90%) at a lower temperature (323 K). Elevating the temperature to 333 K, the selectivity to CMO slightly decreases and HCMA selectivity increases. To further elevate the temperature to 353 K, the CMO selectivity dramatically decreases to 61%, while the quantity of HCMO remarkably increases to 34%. Again, this implies that the CMO is a less thermodynamically stable product although a desired one and it is more difficult to achieve high selectivity to CMO. Besides this, we studied another typical α,β-unsaturated aldehyde, citral hydrogenation over the Pt catalyst. The results indicated that the selectivity has a more remarkable dependence on the reaction temperature (Table S4 in the ESI†). Higher temperature leads to a decrease in the selectivity toward the unsaturated alcohol (C=O bond) and deep hydrogenation to citronellol (the conjugated C=C–C=O bonds). Further study is required to understand the dependence of the catalytic properties on the molecular structure of the substrates.

Regarding the Pt loading, it is found that the CMA conversion decreases with decreasing amount of Pt loading, as shown in Table 4. This is ascribed to the fewer active sites accessible

Table 3 The effect of reaction temperature on the catalytic performance[a]

		Selectivity[b] (%)		
Temp. (K)	Conversion (%)	CMO	HCMA	HCMO
353	97.8	61.3	4.5	34.1
333	79.7	85.4	13.3	1.0
323	61.6	90.5	8.2	0.8

[a] Catalyst: Pt/MA-1. [b] Selectivity was reported at the level of conversion in the table. Reaction conditions: 0.05 g catalyst, substrate: 4 mmol CMA, solvent: 15 mL water, H_2 pressure: 1.0 MPa, reaction time: 2 h.

Table 4 The effect of Pt loading on the catalytic performance[a]

Pt loading[b] (wt%)	Conversion (%)	Selectivity[c] (%)		
		CMO	HCMA	HCMO
1.96	79.7	85.4	13.3	1.0
0.96	63.7	77.2	15.4	6.8
0.47	39.6	70.8	17.6	10.5

[a] Catalyst: Pt/MA-1. [b] As determined by ICP-AES. [c] Selectivity was reported at the level of conversion in the table. Reaction conditions: 0.05 g catalyst, substrate: 4 mmol CMA, solvent: 15 mL water, H_2 pressure: 1.0 MPa, temperature: 333 K, reaction time: 2 h.

for CMA hydrogenation. The CMO selectivity shows an observable decrease from 85% to 71% when the loading ranges from 1.96% to 0.47%. This is not consistent with the results recently reported, where only a marginal variation in CMO selectivity was observed with varied Pt loading.[24] Hence, we observed the Pt particle sizes by TEM. From the TEM results, the decrease in Pt loading leads to a reduction in Pt particle size (Fig. S1 in the ESI†). The catalysts with a Pt loading of 0.96% and 0.47% present a mean Pt particle size of 4.2 and 3.5 nm, respectively. The decrease in selectivity could be explained by the reduced Pt size.

The stability of the supported Pt catalyst was evaluated by recycling in neat water. It is noted that the CMO selectivity still remains at 80% after the fourth use (Fig. 8). The CMA conversion has a marginal decrease from 80% (1st use) to 72% (4th use) mostly owing to a slight leaching of active Pt on the catalysts. The ICP measurement confirmed the amount of Pt loading is 1.86 wt% after the third cycle, slightly lower than that of the initial loading (~1.96 wt%).

In addition, the FTIR and XRD characterization verified that the catalyst is not subject to the structural change after repeated use and no adsorbed species are left over to poison the active Pt (Fig. S2 and S3 in the ESI†). Also, XPS analysis indicated that the Pt species exist in zerovalent form (Pt^0) and is unchanged compared to the catalyst before use (Fig. S4 in the ESI†). Hence, the activity and selectivity remain almost unchanged after repeated use, indicative of their high stability. It is interesting that the HCMA selectivity is little changed even after repeated use. In contrast, the amount of HCMO slightly increases, accompanied by a small decrease in the CMO selectivity after recycling. This proves once again that the transformation from CMO to HCMO could be a main obstacle to be overcome in order to achieve highly selective C=O hydrogenation.

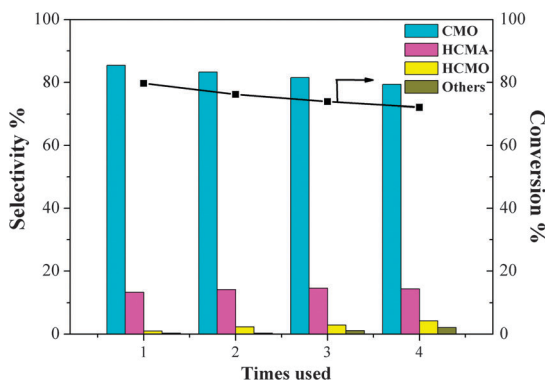

Fig. 8 Recycling use of the supported Pt catalyst in neat water. Reaction conditions: 0.05 g catalyst (Pt/MA-1), substrate: 4 mmol CMA, solvent: 15 mL water, H_2 pressure: 1.0 MPa, temperature: 333 K, reaction time: 2 h.

Conclusions

We have synthesized hydrotalcite-supported Pt catalysts by a solution chemistry method under mild and environmentally benign conditions. The reduction of the metal precursor, the deposition of Pt NCs and the crystallization of the support were achieved in a one-step green process with no involvement of any toxic reagents. The as-synthesized catalysts were applied for hydrogenation of cinnamaldehyde in neat water and showed high selectivity toward CMO (85%) and high activity (TOF 0.488 s^{-1}). The selectivity showed dependence on the size and/or morphology of the Pt NCs. The catalysts can be reused for 4 runs without appreciable loss of activity and decrease of selectivity, indicative of the excellent stability. Particularly, the hydrogenation products could be easily separated from the reaction medium by simple extraction. The organic solvents or toxic agents were completely avoided throughout the preparation and catalytic processes. In addition, the findings suggest that the conversion from CMO to HCMO is a major issue obstructing the achievement of high selectivity toward the C=O bond. This study implies that hydrotalcite-supported Pt NCs are highly selective and stable catalysts for hydrogenation of cinnamaldehyde to a desired unsaturated alcohol by an overall green strategy.

Experimental

Materials

Hexachloroplatinic acid ($H_2PtCl_6{\cdot}6H_2O$, 99.9%) was purchased from Sinopharm Chemical Reagent (Beijing Co. Ltd.). Tetradecyl trimethyl ammonium bromide (TTAB) was obtained from J&K Chemical Co. Ltd. The cinnamaldehyde was purchased from Aldrich Co. Ltd. and used without further purification. The other reagents are of analytical grade. The purity of hydrogen is 99.99%.

Catalyst preparation

$Mg(NO_3)_2{\cdot}6H_2O$ and $Al(NO_3)_3{\cdot}9H_2O$ were dissolved in 30 mL deionized water at room temperature to form a clear salt solution ($[Mg^{2+}]$ = 0.3 M and $[Al^{3+}]$ = 0.1 M, the ratio of Mg/Al = 3 in molar). NaOH and Na_2CO_3 were dissolved in 30 mL deionized water at room temperature to form an alkali solution ($[OH^-]$ = 1.6(Al^{3+} + Mg^{2+}) and CO_3^{2-} = 2$[Al^{3+}]$). The above two solutions were rapidly mixed in a high-speed nucleation reactor for several minutes. Afterwards, the resulting suspension was centrifuged once (4000 rpm, 10 min). The wet precipitate was transferred to a flask, in which 3 mL H_2PtCl_6 (0.0193 M) aqueous solution was diluted to 40 mL and TTAB was added to the solution with an adjustable ratio to Pt metal precursor. The flask was firstly ultrasonicated for 10 min, and then transferred to a temperature-controlled oil bath. After a rapid

addition of ice-cold $NaBH_4$ into the solution ($NaBH_4 : Pt^{4+}$ = 15 : 1 in molar), the flask was capped with a rubber septum and H_2 generated inside was released *via* a needle in the septum for 10 min. Afterwards, the needle was removed and the flask was kept at a constant temperature of 323 K for 6 h. Subsequently, the suspension was centrifuged (4000 rpm, 10 min), washed, and re-dispersed in deionized water for 3 cycles to remove the residues. The solid obtained was dried at 343 K for 12 h before use. The Pt catalysts with reduced loadings (0.96% Pt and 0.47% Pt) were prepared under the same conditions only reducing the amount of H_2PtCl_6 by half or three quarters. The ratio of TTAB to H_2PtCl_6 was kept constant (25 : 1 in molar).

Catalyst characterization

Powder X-ray diffraction (PXRD) measurements. The PXRD patterns of the samples were collected using a Shimadzu XRD-6000 diffractometer (40 kV, 30 mA, graphite-filtered Cu$K\alpha$ radiation, λ = 0.15418 nm).

Elemental analyses. Elemental analyses for metal loadings were performed using an inductively coupled plasma atomic emission spectroscopy (ICP-AES, Shimadzu ICPS-7500).

Fourier-transform infrared spectroscopy measurements. The FTIR spectra of the catalysts were recorded at room temperature using the KBr dilution and pelleting technique on a Bruker Vector 22 spectrometer in the range 4000–400 cm^{-1} at a 4 cm^{-1} resolution.

Transmission electron microscopy (TEM) analyses. TEM photographs were taken using a JEOL JEM-2100 microscope. For TEM observations, the samples were ultrasonically dispersed in ethanol and a drop of the suspension was deposited on a carbon-coated Cu grid followed by the evaporation of solvent in air.

X-ray photoelectron spectra (XPS) measurements. The XPS spectra of catalysts were recorded on a Thermo VG ESCALAB250 X-ray photoelectron spectrometer at a pressure of about 2×10^{-9} Pa using Al $K\alpha$ X-ray as the excitation source (1486.6 eV). The shifts of all binding energies were calibrated using C1s core level at 284.6 eV.

Nitrogen adsorption–desorption measurements. The specific surface areas were measured from N_2-adsorption at 77 K using a static volumetric Quantachrome Autosorb-1C-VP Analyzer. The specific surface area was calculated using a BET method.

CO-adsorption infrared analyses. The FTIR of CO-adsorption was achieved on a PC-controlled PWP 110-40 FTIR spectrophotometer. A catalyst of ~30 mg was pressed into a self-supporting pellet and placed in a sealed chamber. The chamber was purged with a flow of highly-pure N_2 and heated to 343 K and maintained for 1 h. After the pretreatment, the chamber was cooled down to 298 K under a N_2 atmosphere. Subsequently, highly pure CO gas was introduced to achieve the adsorption of CO molecules onto the catalysts. Afterwards, the chamber was re-purged by N_2 to drive the CO in the gas phase away. The IR spectra were recorded by averaging 64 scans with a resolution of 2 cm^{-1}.

Catalytic tests

General procedure for the hydrogenation of cinnamaldehyde. The catalytic tests were carried out in a magnetically stirred autoclave (100 mL, Parr-5000). The stirring rate was sufficiently high to minimize the mass transfer effect. The catalyst (0.05 g) was firstly added to 15 mL of solvent. The cinnamaldehyde (4×10^{-3} mol) was injected into the solvent. The autoclave was repeatedly flushed with H_2 for 10 times before reaction. The autoclave was placed in a heating jacket and preheated to a reaction temperature of 333 K. Then it was pressurized to total H_2 pressure of 1.0 MPa. Zero reaction time was recorded while the autoclave was pressurized to the desired H_2 pressure and the reactions typically lasted for 2 h. The products were analyzed using a gas chromatograph (Agilent 7890A) with a HP-5 capillary column attached to a flame ionization detector (FID). In order to reveal the role of alkali as a promoter, NaOH of 0.01g (0.25 mmol) was added to the reaction solvent (water of 15 mL). The catalytic reactions were carried out in the presence of alkali.

Recovery and reuse of the supported Pt catalysts. The catalyst was collected after filtration washed with acetone three times and then with distilled water several times. The catalyst was then dried at 343 K for 12 h before being used for the next run.

Abbreviations

UALs	α,β-Unsaturated aldehydes
UKEs	α,β-Unsaturated ketones
CMA	Cinnamaldehyde
CMO	Cinnamyl alcohol
HCMA	Hydrocinnamaldehyde
HCMO	Phenyl propanol

Acknowledgements

The authors acknowledge the financial support from the National Natural Science Foundation of China (Grant no. 21076016), the Program for Changjiang Scholars and Innovative Research Team in University (Grant no. IRT1205), the 973 Program (Grant no. 2011CBA00506) and the fund of the Key Laboratory of Fine Petrochemical Engineering of Jiangsu Province.

Notes and references

1 R. L. Augustine, in *Heterogeneous Catalysts in Organic Synthesis*, ed. Dekker, New York, 1995.
2 B. Coq and F. Figueras, *Coord. Chem. Rev.*, 1998, **1753**, 178.
3 D. Y. Murzin, P. Maki-Arvela, J. Hajek and T. Salmi, *Appl. Catal., A*, 2005, **292**, 1.
4 D. Loffreda, F. Delbecq, F. Vigné and P. Sautet, *J. Am. Chem. Soc.*, 2006, **128**, 1316.
5 M. S. Ide, B. Hao, M. Neurock and R. J. Davis, *ACS Catal.*, 2012, **2**, 671.
6 X. Zhang, Y. C. Guo, Z. C. Zhang, J. S. Gao and C. M. Xu, *J. Catal.*, 2012, **292**, 213.
7 J. Hidalgo-Carrillo, M. A. Aramendía, A. Marinas, J. M. Marinas and F. J. Urbano, *Appl. Catal., A*, 2010, **385**, 190.

8 C.-Y. Hsu, T.-C. Chiu, M.-H. Shih, W.-J. Tsai, W.-Y. Chen and C.-H. Lin, *J. Phys. Chem. C*, 2010, **114**, 4502.
9 J. P. Tessonnier, L. Pesant, G. Ehret, M. J. Ledoux and C. Pham-Huu, *Appl. Catal., A*, 2005, **288**, 203.
10 B. C. Campo, M. A. Volpe and C. E. Gigola, *Ind. Eng. Chem. Res.*, 2009, **48**, 10234.
11 J. Zhu, M. Li, M. Lu and J. Zhu, *Catal. Sci. Technol.*, 2013, **3**, 737.
12 J. Álvarez-Rodríguez, I. Rodríguez-Ramos, A. Guerrero-Ruiz and A. Arcoya, *Appl. Catal., A*, 2009, **366**, 114.
13 A. K. Prashar, S. Mayadevi and R. Nandini Devi, *Catal. Commun.*, 2012, **28**, 42.
14 J. C. Serrano-Ruiz, A. López-Cudero, J. Solla-Gullón, A. Sepúlveda-Escribano, A. Aldazb and F. Rodríguez-Reinoso, *J. Catal.*, 2008, **253**, 159.
15 X. Han, R. Zhou, B. Yue and X. Zheng, *Catal. Lett.*, 2006, **109**, 157.
16 Y. Li, P. F. Zhu and R. X. Zhou, *Appl. Surf. Sci.*, 2008, **254**, 2609.
17 Y. Li, Z. G. Li and R. X. Zhou, *J. Mol. Catal. A: Chem.*, 2008, **279**, 140.
18 Z. Guo, Y. Chen, L. Li, X. Wang, G. L. Haller and Y. Yang, *J. Catal.*, 2010, **276**, 314.
19 K. Q. Sun, Y. C. Hong, G. R. Zhang and B. Q. Xu, *ACS Catal.*, 2011, **1**, 1336.
20 Rodiansono, S. Khairi, T. Hara, N. Ichikuni and S. Shimazu, *Catal. Sci. Technol.*, 2012, **2**, 2139.
21 M. L. Toebes and Y. H. Zhang, *J. Catal.*, 2004, **226**, 215.
22 A. Sepulveda-Escribano, E. V. Ramos-Fernandez and F. Rodriguez-Reinoso, *Catal. Commun.*, 2008, **9**, 1243.
23 E. V. Ramos-Fernández, J. Ruiz-Martínez, J. C. Serrano-Ruiz, J. Silvestre-Albero, A. Sepúlveda-Escribano and F. Rodríguez-Reinoso, *Appl. Catal., A*, 2011, **402**, 50.
24 S. Bhogeswararao and D. Srinivas, *J. Catal.*, 2012, **285**, 31.
25 A. Rajagopalan and W. Kroutil, *Mater. Today*, 2011, **14**, 144.
26 P. Barbaro, L. Gonsalvi, A. Guerriero and F. Liguori, *Green Chem.*, 2012, **14**, 3211.
27 X. Wu, J. Liu, X. Li, A. Zanotti-Gerosa, F. Hancock, D. Vinci, J. Ruan and J. Xiao, *Angew. Chem., Int. Ed.*, 2006, **45**, 6718.
28 I. T. Horvaeth, *Green Chem.*, 2008, **10**, 1024.
29 B. H. Zhao, J. G. Chen, X. Liu, Z. W. Liu, Z. Hao, J. Xiao and Z. T. Liu, *Ind. Eng. Chem. Res.*, 2012, **51**, 11112.
30 J. Zhu, Y. Jia, M. Li, M. Lu and J. Zhu, *Ind. Eng. Chem. Res.*, 2013, **52**, 1224.
31 M. M. Wang, L. He, Y. M. Liu, Y. Cao, H. Y. He and K. N. Fan, *Green Chem.*, 2011, **13**, 602.
32 D. Tongsakul, S. Nishimura, C. Thammacharoen, S. Ekgasit and K. Ebitani, *Ind. Eng. Chem. Res.*, 2012, **51**, 16182.
33 F. Zhang, X. Zhao, C. Feng, B. Li, T. Chen, W. Lu, X. Lei and S. Xu, *ACS Catal.*, 2011, **1**, 232.
34 B. M. Choudary, S. Madhi, N. S. Chowdari, M. L. Kantamn and B. Sreedhar, *J. Am. Chem. Soc.*, 2002, **124**, 14127.
35 D. G. Li, C. Wang, D. Tripkovic, S. Sun, N. M. Markovic and V. R. Stamenkovic, *ACS Catal.*, 2012, **2**, 1358.
36 M. Ogawa and H. Kaiho, *Langmuir*, 2002, **18**, 4240.
37 C. K. Tsung, J. N. Kuhn, W. Huang, C. Aliaga, L.-I. Hung, G. A. Somorjai and P. Yang, *J. Am. Chem. Soc.*, 2009, **131**, 5816.
38 K. M. Bratlie, H. Lee, K. Komvopoulos, P. Yang and G. A. Somorjai, *Nano Lett.*, 2007, **7**, 3097.
39 S. C. Tsang, N. Cailuo, W. Oduro, A. T. S. Kong, L. Clifton, K. M. K. Yu, B. Thiebaut, J. Cookson and P. Bishop, *ACS Nano*, 2008, **2**, 2547.
40 P. Bera, K. R. Priolkar and A. Gayen, *Chem. Mater.*, 2003, **15**, 2049.
41 L. Charles de Menorval, A. Chaqroune, B. Coq and F. Figueras, *J. Chem. Soc., Faraday Trans.*, 1997, **93**, 3715.
42 M. Boronat and A. Corma, *Langmuir*, 2010, **26**, 16607.
43 H. G. Manyar, D. Weber, H. Daly, J. M. Thompson, D. W. Rooney, L. F. Gladden, E. Hugh Stitt, J. Jose Delgado, S. Bernal and C. Hardacre, *J. Catal.*, 2009, **265**, 80.
44 Z. Tian, X. Xiang, L. Xie and F. Li, *Ind. Eng. Chem. Res.*, 2013, **52**, 288.
45 P. Gallezot and D. Richard, *Catal. Rev. Sci. Eng.*, 1998, **40**, 81.
46 W. Yu, H. Liu, M. Liu and Q. Tao, *J. Mol. Catal. A: Chem.*, 1999, **138**, 273.